

000 001 002 003 004 005 006 007 008 009 010 011 012 013 014 015 016 017 018 019 020 021 022 023 024 025 026 027 028 029 030 031 032 033 034 035 036 037 038 039 040 041 042 043 044 045 046 047 048 049 050 051 052 053 MODEL ALREADY KNOWS THE BEST NOISE: BAYESIAN ACTIVE NOISE SELECTION VIA ATTENTION IN VIDEO DIFFUSION MODEL

Anonymous authors

Paper under double-blind review

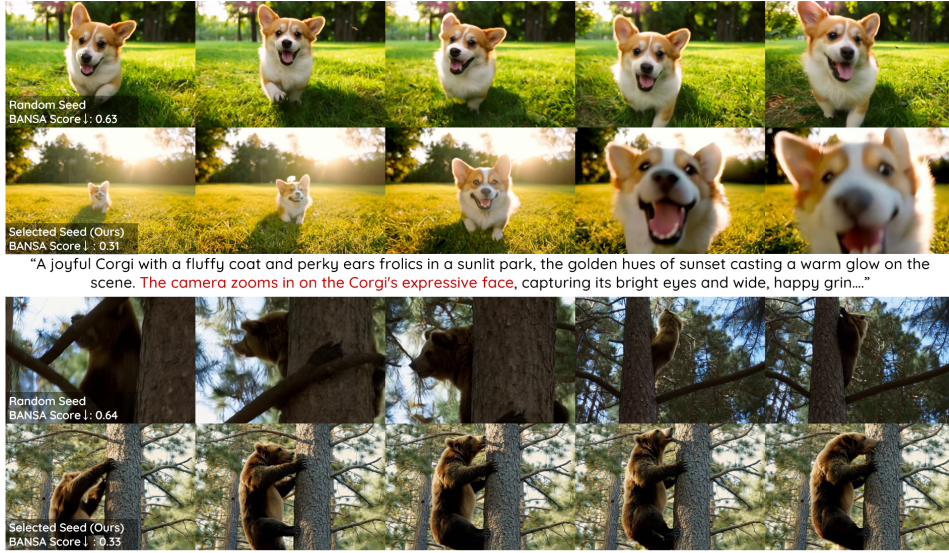


Figure 1: **Random Seed vs. Ours.** We propose ANSE, a noise selection framework, and the BANSA Score, an uncertainty-based metric. By selecting initial noise seeds with lower BANSA scores, which indicate more certain noise samples, ANSE improves video generation performance.

ABSTRACT

The choice of initial noise strongly affects quality and prompt alignment in video diffusion; different seeds for the same prompt can yield drastically different results. While recent methods use externally designed priors (e.g., frequency filtering or inter-frame smoothing), they often overlook internal model signals that indicate inherently preferable seeds. To address this, we propose **ANSE** (Active Noise Selection for Generation), a model-aware framework that selects high-quality seeds by quantifying attention-based uncertainty. At its core is **BANSA** (Bayesian Active Noise Selection via Attention), an acquisition function that measures entropy disagreement across multiple stochastic attention samples to estimate model confidence and consistency. For efficient inference-time deployment, we introduce a Bernoulli-masked approximation of BANSA that estimates scores from a single diffusion step and a subset of informative attention layers. Experiments across diverse text-to-video backbones demonstrate improved video quality and temporal coherence with marginal inference overhead, providing a principled and generalizable approach to noise selection in video diffusion. See our project page: <https://anse-anonymous.vercel.app/>.

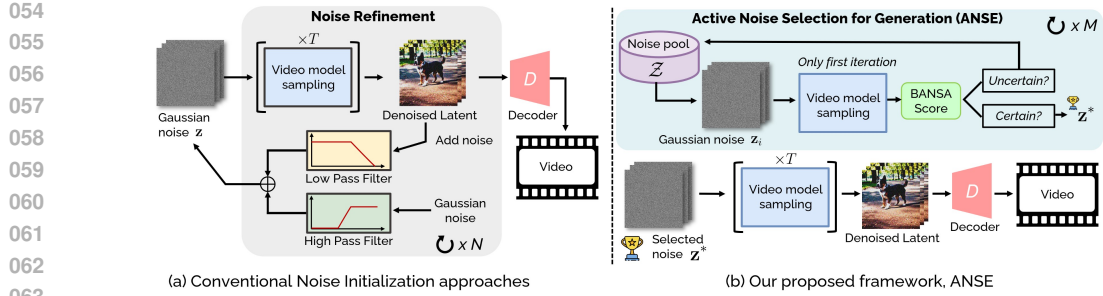


Figure 2: **Conceptual comparison of noise initialization.** (a) Prior methods (Wu et al., 2024; Yuan et al., 2025) refine noise via frequency priors and full diffusion sampling, leading to high cost. (b) Our method instead selects noise seeds by estimating attention-based uncertainty at the first denoising step, enabling efficient, model-aware selection.

1 INTRODUCTION

Diffusion models have rapidly established themselves as a powerful class of generative models, demonstrating state-of-the-art performance across images and videos (Rombach et al., 2022; Esser et al., 2024; Xie et al., 2024; Chen et al., 2024b;a; Wang et al., 2025; Yang et al., 2024; Zheng et al., 2024; Team, 2025). In particular, Text-to-Video (T2V) diffusion models have received increasing attention for their ability to generate temporally coherent and visually rich video sequences. To achieve this, most T2V model architectures extend Text-to-Image (T2I) diffusion backbones by incorporating temporal modules or motion-aware attention layers (Blattmann et al., 2023; He et al., 2022; Wang et al., 2023; Chen et al., 2023; 2024a; Guo et al., 2024b; Wang et al., 2025). Furthermore, other works explore video generative structures, such as causal autoencoders or video autoencoder-based models, which aim to generate full video volumes rather than a sequence of independent frames (Hong et al., 2022; Yang et al., 2024; HaCohen et al., 2024; Kong et al., 2024; Zheng et al., 2024; Team, 2025).

Beyond architectural design, another promising direction lies in improving noise initialization at inference time for T2I and T2V generation (Guo et al., 2024a; Eyring et al., 2024; Chen et al., 2024c; Xu et al., 2025). This aligns with the growing trend of inference-time scaling, observed not only in Large Language Models (Brown et al., 2024; Snell et al., 2024) but also in diffusion-based generation systems (Ma et al., 2025). Due to the iterative nature of the diffusion process, the choice of initial noise profoundly influences video quality, temporal consistency, and prompt alignment (Ge et al., 2023; Wu et al., 2024; Qiu et al.; Yuan et al., 2025). As illustrated in Figure 1, the same prompt can lead to drastically different videos depending solely on the noise seed, motivating the need for intelligent noise selection.

Recent approaches tackle this by introducing external noise priors. PYoCo (Ge et al., 2023) enforces inter-frame dependent patterns for coherence but requires heavy fine-tuning. FreeNoise (Qiu et al.) reschedules noise across time with a fusion strategy, FreeInit (Wu et al., 2024) preserves low-frequency components via frequency filtering, and FreqPrior (Yuan et al., 2025) extends this with Gaussian-shaped priors and partial sampling. While effective, these methods rely on external priors and repeated full diffusion passes, while ignoring internal model signals that identify inherently preferable seeds.

To address this limitation, we propose a model-aware noise selection framework, **ANSE** (Active Noise Selection for Generation), grounded in Bayesian uncertainty. At the core of ANSE is **BANSA** (Bayesian Active Noise Selection via Attention), an acquisition function that identifies noise seeds inducing confident and consistent attention behaviors under stochastic perturbations. A conceptual comparison between our method and prior frequency-based approaches is illustrated in Figure 2, highlighting the difference between external priors and model-informed uncertainty estimates.

Unlike BALD (Gal et al., 2017), which estimates uncertainty from classification logits, BANSA measures entropy in attention maps, arguably the most informative signals in diffusion. It compares the mean of per-pass entropies with the entropy of the mean map, capturing both uncertainty and cross-pass disagreement. A lower BANSA score indicates more confident, consistent attention and empirically correlates with more coherent video generation (Fig. 1). To make BANSA inference-

friendly, we approximate it with Bernoulli-masked attention, yielding multiple stochastic attention samples from a single forward pass. We further cut cost by evaluating early denoising steps and only a subset of informative layers selected via correlation analysis. Our contributions are threefold:

- We present **ANSE**, the first active noise selection framework for video diffusion, grounded in a Bayesian formulation of attention-based uncertainty.
- We introduce **BANSA**, an acquisition function that measures attention consistency under stochastic perturbations, enabling model-aware noise selection without retraining.
- Our method improves video quality and temporal consistency across diverse text-to-video backbones, with only marginal inference overhead.

2 PRELIMINARY

Video Diffusion Models Diffusion models (Ho et al., 2020; Song et al., 2021b) have achieved strong results across generative tasks. In T2V, pixel-space diffusion is costly, so most video diffusion models adopt latent diffusion and operate in a compressed latent space. A video autoencoder with encoder \mathcal{E} and decoder \mathcal{D} reconstructs \mathbf{x} as $\mathbf{x} = \mathcal{D}(\mathcal{E}(\mathbf{x}))$. Let $\mathbf{z}_0 = \mathcal{E}(\mathbf{x})$. The forward diffusion then progressively adds noise over time:

$$\mathbf{z}_t = \sqrt{\bar{\alpha}_t} \mathbf{z}_0 + \sqrt{1 - \bar{\alpha}_t} \boldsymbol{\epsilon}, \quad \boldsymbol{\epsilon} \sim \mathcal{N}(0, \mathbf{I}), \quad t = 1, \dots, T,$$

where $\bar{\alpha}_t$ is a pre-defined variance schedule. To learn the reverse process, a denoising network ϵ_θ is trained using the denoising score matching loss (Vincent, 2011):

$$\mathcal{L}_\theta = \mathbb{E}_{\mathbf{z}_t, \boldsymbol{\epsilon}, t} \left[\|\epsilon_\theta(\mathbf{z}_t, \mathbf{c}, t) - \boldsymbol{\epsilon}\|^2 \right],$$

where \mathbf{c} is the conditioning text. Sampling starts from Gaussian noise $\mathbf{z}_T \sim \mathcal{N}(0, \mathbf{I})$ and uses a deterministic DDIM solver (Song et al., 2021a). Each step updates as:

$$\mathbf{z}_{t-1} = \sqrt{\bar{\alpha}_t} \hat{\mathbf{z}}_0(t) + \sqrt{1 - \bar{\alpha}_{t-1}} \epsilon_\theta(\mathbf{z}_t, \mathbf{c}, t),$$

where the denoised latent estimate $\hat{\mathbf{z}}_0(t) := \frac{\mathbf{z}_t - \sqrt{1 - \bar{\alpha}_t} \epsilon_\theta(\mathbf{z}_t, \mathbf{c}, t)}{\sqrt{\bar{\alpha}_t}}$ is obtained using Tweedie's formula (Efron, 2011; Kim & Ye, 2021). This iterative process continues until $t = 1$, yielding the final denoised latent \mathbf{z}_0 , which is decoded into a video via \mathcal{D} .

Bayesian Active Learning by Disagreement (BALD) Active learning selects the most informative samples from an unlabeled pool to improve training. Acquisition functions are commonly uncertainty-based (Houlsby et al., 2011; Gal et al., 2017; Kirsch et al., 2019; Yoo & Kweon, 2019) or distribution-based (Mac Aodha et al., 2014; Yang et al., 2015; Sener & Savarese, 2017; Sinha et al., 2019), and some use external modules such as auxiliary predictors (Yoo & Kweon, 2019; Tran et al., 2019; Kim et al., 2021). While most prior work targets image classification, we adapt uncertainty-based acquisition to text-to-video generation without additional models.

Predictive entropy is widely used, but it reflects data noise and does not isolate parameter uncertainty. BALD instead measures *epistemic* uncertainty via the mutual information between predictions \mathbf{y} and parameters θ :

$$\text{BALD}(\mathbf{x}) = \mathcal{H}[p(\mathbf{y}|\mathbf{x})] - \mathbb{E}_{p(\theta|\mathcal{D}_U)} [\mathcal{H}[p(\mathbf{y}|\mathbf{x}, \theta)]], \quad (1)$$

where $\mathcal{H}[p] = -\sum_y p(y) \log p(y)$ is Shannon entropy (Shannon, 1948). The first term is the entropy of the mean prediction, and the second is the average entropy across stochastic forward passes. A high BALD score means predictions are confident yet disagree, indicating high epistemic uncertainty. Since the posterior over θ is intractable, BALD is approximated using K stochastic forward passes (e.g., Monte Carlo dropout):

$$\widehat{\text{BALD}}(\mathbf{x}) = \mathcal{H} \left[\frac{1}{K} \sum_{k=1}^K p^{(k)}(\mathbf{y}|\mathbf{x}) \right] - \frac{1}{K} \sum_{k=1}^K \mathcal{H} \left[p^{(k)}(\mathbf{y}|\mathbf{x}) \right]. \quad (2)$$

We reinterpret BALD for inference-time generative modeling. Rather than selecting samples for labeling, we apply BALD to rank noise seeds by their epistemic uncertainty. Selecting seeds with lower BALD scores results in more stable model behavior and leads to higher-quality generations.

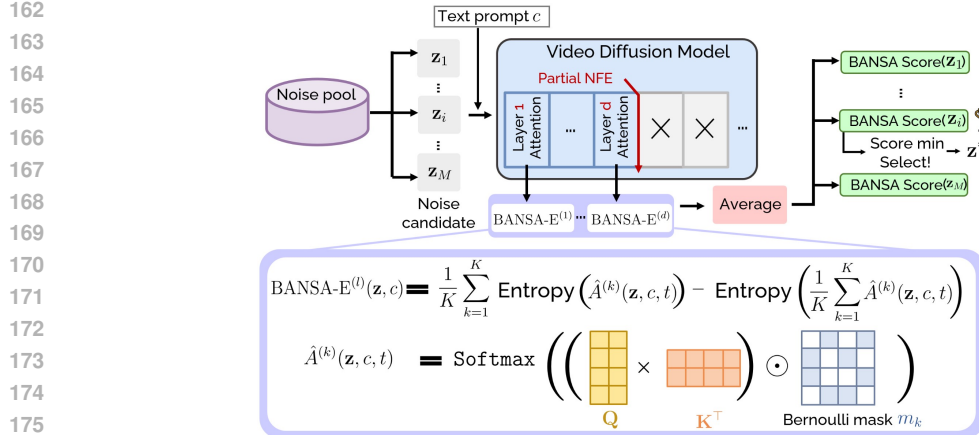


Figure 3: **Overview of our BANSA-based noise selection process.** Given a text prompt c , we compute BANSA scores for multiple noise seeds $\{z_1, \dots, z_M\}$ using Bernoulli-masked attention maps from selected layers at an early diffusion step. The seed with the lowest score, indicating confident and consistent attention, is selected for generation.

3 METHODS

We propose **ANSE**, a framework for selecting high-quality noise seeds in T2V diffusion based on model uncertainty (Fig. 2). ANSE centers on **BANSA**, an acquisition function that transfers uncertainty criteria from classification to the attention space of generative diffusion models (Sec. 3.1). For efficient inference, we approximate BANSA via Bernoulli-masked attention sampling (Sec. 3.2). To avoid redundancy, we select a representative attention layer using correlation-based linear probing (Sec. 3.3). The full pipeline appears in Fig. 3.

3.1 BANSA: BAYESIAN ACTIVE NOISE SELECTION VIA ATTENTION

We introduce **BANSA**, an acquisition function for selecting optimal noise seeds in T2V diffusion. Unlike classifiers with explicit predictive distributions, diffusion models do not expose such outputs, so we estimate uncertainty in the attention space where text and visual tokens align during generation. We treat attention maps as stochastic predictions conditioned on the seed z , prompt c , and timestep t . BANSA measures both disagreement and confidence across multiple attention samples, providing a BALD-style uncertainty criterion tailored to the generative setting.

Definition 1 (BANSA Score). *Let z be a noise seed, c a text prompt, and t a diffusion timestep. Let $\mathbf{Q}(z, c, t), \mathbf{K}(z, c, t) \in \mathbb{R}^{N \times d}$ denote the query and key matrices from a denoising network ϵ_θ . The attention map is computed as:*

$$A(z, c, t) := \text{Softmax}(\mathbf{Q}(z, c, t) \mathbf{K}(z, c, t)^\top) \in \mathbb{R}^{N \times N}. \quad (3)$$

*Let $\mathcal{A}(z, c, t) = \{A^{(1)}, \dots, A^{(K)}\}$ denote a set of K stochastic attention maps obtained via forward passes with random perturbations (e.g., Bernoulli masking). The **BANSA score** is defined as:*

$$\text{BANSA}(z, c, t) := \mathcal{H}\left(\frac{1}{K} \sum_{k=1}^K A^{(k)}\right) - \frac{1}{K} \sum_{k=1}^K \mathcal{H}(A^{(k)}), \quad (4)$$

where $\mathcal{H}(A) := \frac{1}{N} \sum_{i=1}^N \sum_{j=1}^N -A_{ij} \log A_{ij}$. This formulation captures both the sharpness (confidence) and the consistency (agreement) of attention behavior. BANSA can be applied to various attention types (e.g., cross-, self-, or temporal) and allows layer-wise interpretability.

Given a noise pool $\mathcal{Z} = \{z_1, \dots, z_M\}$, we select the optimal noise seed that minimizes score:

$$z^* := \arg \min_{z \in \mathcal{Z}} \text{BANSA}(z, c, t). \quad (5)$$

A desirable property of BANSA is that its score becomes zero when all attention samples are identical, reflecting complete agreement and certainty. We formalize this as follows:

216 **Algorithm 1:** Active Noise Selection with BANSA Score for Video Generation

217 **Input:** Text prompt c , noise pool $\mathcal{Z} = \{\mathbf{z}_1, \dots, \mathbf{z}_M\}$, timestep t , cutoff layer d^*

218 1 **foreach** $\mathbf{z}_i \in \mathcal{Z}$ **do**

219 2 | Compute BANSA score: $\widehat{\text{BANSA-E}}_{\leq d^*}(\mathbf{z}_i, c, t)$ via Eq. (7);

220 3 | Select optimal noise: $\mathbf{z}^* = \arg \min_{\mathbf{z}_i} \widehat{\text{BANSA-E}}_{\leq d^*}(\mathbf{z}_i, c, t)$;

221 4 **return** Generate video: $\hat{v} = \text{SampleVideo}(\mathbf{z}^*, c, t)$;

225 **Proposition 1** (BANSA Zero Condition). *Let $\mathcal{A}(\mathbf{z}, c, t) = \{A^{(1)}, \dots, A^{(K)}\}$ be a set of row-stochastic attention maps. Then:*

$$\text{BANSA}(\mathbf{z}, c, t) = 0 \Leftrightarrow A^{(1)} = \dots = A^{(K)}.$$

229 The proof is deferred to the Appendix B. This result implies that minimizing the BANSA score
230 encourages attention that is both confident and consistent under stochastic perturbations. Empirically,
231 low BANSA correlates with better prompt alignment, temporal coherence, and visual fidelity. Thus,
232 BANSA provides a principled, model-aware criterion for noise selection in T2V.

234 3.2 STOCHASTIC APPROXIMATION OF BANSA VIA BERNOUlli-MASKED ATTENTION

236 While BANSA is principled for noise selection, computing it with K independent passes per seed \mathbf{z}
237 is costly. We instead draw K stochastic attention samples from a *single* pass via Bernoulli-masked
238 attention. Rather than running K passes, we inject stochasticity directly into the attention scores. For
239 each $k = 1, \dots, K$, sample a binary mask $m_k \in \{0, 1\}^{N \times N}$ i.i.d. from Bernoulli(p) and compute
240 masked attention map, $\hat{A}^{(k)}(\mathbf{z}, c, t) := A(\mathbf{z}, c, t) \odot m_k$, \odot denotes element-wise multiplication and
241 rows are re-normalized. Using these K such samples, we define the approximate BANSA:

$$\text{BANSA-E}(\mathbf{z}, c, t) := \mathcal{H} \left(\frac{1}{K} \sum_{k=1}^K \hat{A}^{(k)}(\mathbf{z}, c, t) \right) - \frac{1}{K} \sum_{k=1}^K \mathcal{H}(\hat{A}^{(k)}(\mathbf{z}, c, t)). \quad (6)$$

245 By concavity of entropy, $\text{BANSA-E} \geq 0$. Although approximate, it efficiently captures attention-level
246 epistemic uncertainty and serves as a practical surrogate for model-aware noise selection.¹ As shown
247 in Table 4, experimental validation confirms that this method is sufficient for selecting optimal noisy
248 samples from the model’s perspective.

249 3.3 LAYER SELECTION VIA CUMULATIVE BANSA CORRELATION

252 BANSA can be computed at any layer, but behavior differs across depth. Using all layers is costly, so
253 we truncate at the smallest depth d^* where the average BANSA up to d remains highly correlated
254 with the full-layer score. Given a noise seed $\mathbf{z}_i \in \mathcal{Z} = \{\mathbf{z}_1, \dots, \mathbf{z}_M\}$ and L attention layers, we
255 compute per-layer scores $\text{BANSA-E}^{(l)}(\mathbf{z}_i, c, t)$ and define the cumulative average up to layer d as:

$$\widehat{\text{BANSA-E}}_{\leq d}(\mathbf{z}_i, c, t) := \frac{1}{d} \sum_{l=1}^d \text{BANSA-E}^{(l)}(\mathbf{z}_i, c, t). \quad (7)$$

259 To find d^* , we compute the Pearson correlation (Pearson, 1895) between the partial average
260 $\widehat{\text{BANSA-E}}_{\leq d}$ and the full-layer average $\widehat{\text{BANSA-E}}_{\leq L}$, and choose the smallest d such that
261 $\text{Corr}(\widehat{\text{BANSA-E}}_{\leq d}, \widehat{\text{BANSA-E}}_{\leq L}) \geq \tau$. We validate this procedure using 100 prompts and 10
262 noise seeds across all evaluated models as detailed in Appendix D. As shown in Figure 7, the correla-
263 tion quickly stabilizes at a moderate depth, allowing us to select d^* without using all layers. We then
264 define the BANSA score as $\widehat{\text{BANSA-E}}_{\leq d^*}$ to guide noise selection, as summarized in Algorithm 1.
265 With d^* fixed per model, it adds no runtime cost, and $\widehat{\text{BANSA-E}}_{\leq d^*}$ (truncated layer) consistently
266 matches the full-layer score and robustly preserves generation quality across models, confirming its
267 reliability as a practical surrogate as shown Appendix D and E (see detail).

268
269 ¹We use “Bayesian” in the sense of epistemic uncertainty estimation, following BALD (Houlsby et al., 2011),
rather than a full posterior derivation.

270

4 ANALYSIS OF BANSA-SELECTED NOISE

271
 272 In this section, we aim to investigate the property of noise seeds selected by BANSA, and consist of
 273 three experiments which declare our framework and interpret the noise seeds. Our framework does
 274 not seek a universal “golden” seed, but selects the most suitable one for each prompt by minimizing
 275 uncertainty. The effectiveness of a noise seed is therefore *prompt-dependent*: a seed that improves
 276 one prompt may degrade another.

277 **Experiment 1: Cross-Prompt Behavior.** To Table 1: Cross-prompt evaluation of a high-
 278 demonstrate this prompt-dependent behavior, We BANSA seed from A.
 279 select a high-BANSA (worst-performing) seed
 280 from prompt A and applied it to prompts B and C
 281 (Table 1) and measures Subject and Background
 282 Consistency. The seed degraded quality for prompt
 283 C but improved performance for prompt B, con-
 284 firming that noise effectiveness depends on prompt context rather than intrinsic seed quality.

285 While Experiment 1 shows how noise effectiveness varies across prompts, the following two experi-
 286 ments examine whether similar patterns also emerge within a *fixed* prompt.

287 **Experiment 2: Intra-Prompt Attention Consis- Table 2: Pairwise distances within attention
 288 tency.** To examine whether BANSA uncertainty re- maps.

289 lates to attention stability, we generate five samples
 290 per prompt (total 100 prompts), selected the highest-
 291 and lowest-scoring seeds, and computed pairwise Eu-
 292 clidean distances between their attention maps (Ta-
 293 ble 2). Low-BANSA seeds showed smaller intra-group distances, indicating more stable and consis-
 294 tent patterns, while high-BANSA seeds exhibited higher variability.

295 **Experiment 3: Latent Trajectory and Expressiveness.** Table 3: Latent stability and visual dy-
 296 Beyond attention maps, we further investigate latent-space
 297 dynamics. Across 100 prompts with five repetitions each,
 298 we compare high- and low-BANSA seeds over all denoising
 299 steps (Table 3). We measured two metrics: (1) Latent
 300 Trajectory Variation, obtained by applying a Butterworth
 301 low-pass filter to isolate low-frequency structural compo-
 302 nents (Wu et al., 2024; Yuan et al., 2025) and computing their temporal variation, where lower values
 303 indicate smoother and more stable trajectories; and (2) Intra-frame Variance, the average spatial
 304 variance within frames, where higher values indicate richer dynamic expressiveness. Low-BANSA
 305 seeds showed both lower trajectory variation and higher intra-frame variance, combining temporal
 306 stability with more expressive video generation.

307 **Takeaway and Relation to Prior Work.** The three findings indicate that BANSA identifies seeds
 308 with lower uncertainty, leading to (1) prompt-specific improvements, (2) more stable attention, and
 309 (3) smoother yet more expressive latent dynamics. This is consistent with FreeInit Wu et al. (2024)
 310 and FreeQPrior (Yuan et al., 2025), which emphasize stable latent initialization and low-frequency
 311 structure. BANSA complements these insights by offering an uncertainty-driven selector that explains
 312 why such seeds generalize within a prompt while remaining prompt-dependent across prompts.

313

5 EXPERIMENTS

316 **Experimental Setting.** We evaluate **ANSE** on diverse T2V diffusion backbones—AnimateDiff (Guo
 317 et al., 2024b), CogVideoX-2B/5B (Yang et al., 2024), Wan2.1 (Team, 2025), and Hunyuan-
 318 Video (Kong et al., 2024). To rigorously evaluate our method, we follow each model’s official
 319 sampling protocol; for resolution, Wan2.1 is evaluated at 480p and HunyuanVideo at 360p due to
 320 resource limits. Results for noise-prior refinement baselines (FreqPrior (Yuan et al., 2025)) are
 321 reported only on AnimateDiff, as they lack official support on the others and incur $\sim 3\times$ inference
 322 time. ANSE is orthogonal and can be combined with these priors. Unless noted, we use a noise pool
 323 of $M=10$ with $K=10$ stochastic passes per seed, and Bernoulli-masked attention with $p=0.2$. All
 experiments run on NVIDIA H100 GPUs. Further details are in the Appendix C.

324 Table 4: Quantitative results on VBench using AnimateDiff, CogVideoX-2B and -5B.
325

Backbone Model	Method	Quality Score	Semantic Score	Total Score	Inference Time
AnimateDiff (Guo et al., 2024b)	Vanilla	80.22	69.03	77.98	28.23s
	+ Ours	81.66	71.09	79.33	31.33s _(+10.98%)
	Freqprior	81.22	70.45	79.07	58.01 _(+105.36%)
	+ Ours	82.23	73.23	80.43	61.12s _(+5.36%)
CogVideoX-2B (Yang et al., 2024)	Vanilla	82.08	76.83	81.03	247.8s
	+ Ours	82.56	78.06	81.66	269.3s _(+8.67%)
CogVideoX-5B (Yang et al., 2024)	Vanilla	82.53	77.50	81.52	667.3s
	+ Ours	82.70	78.10	81.71	754.1s _(+13.1%)

335 Table 5: Quantitative results on quality score metrics for HunyuanVideo and Wan2.1
336

Backbone Model	Method	Subject Consistency ↑	Background Consistency ↑	Motion Smoothness ↑	Aesthetic Quality ↑	Imaging Quality ↑	Temporal Flickering ↑	Inference Time ↓
HunyuanVideo (Kong et al., 2024)	Vanilla	0.9562	0.9656	0.9850	0.6276	0.6137	0.9921	52.3s
	+ Ours	0.9612	0.9661	0.9858	0.6268	0.6151	0.9938	59.8s _(+14.34%)
Wan2.1 (Team, 2025)	Vanilla	0.9562	0.9656	0.9850	0.6276	0.6137	0.9943	43.8s
	+ Ours	0.9612	0.9661	0.9858	0.6268	0.6151	0.9956	50.7s _(+15.75%)

341 **Evaluation Metric.** We evaluate with VBench (Huang et al., 2024), which reports a quality score
342 and a semantic score, combined into a total score on a 0–100 scale. For AnimateDiff and CogVideoX-
343 2B/5B, we report both quality and semantic scores. For HunyuanVideo and Wan2.1, we restrict
344 evaluation to the six quality dimensions due to computational constraints, while noting that semantic
345 evaluation can also be applied in principle. All reported results are obtained by repeating each
346 evaluation dimension five times and averaging the scores.

347 **Quantitative Comparison.** As shown in Table 4, ANSE consistently improves performance across
348 diverse T2V backbones. On AnimateDiff, ANSE outperforms the vanilla baseline and further
349 demonstrates clear advantages over noise-initialization methods such as FreqPrior (Yuan et al., 2025).
350

351 Notably, ANSE is also fully compatible with FreqPrior, achieving even higher scores when combined.
352 Table 4 also reports results on CogVideoX-2B and -5B, which adopt the more advanced MMDiT ar-
353 chitecture. ANSE improves quality, semantic, and total VBench scores on both scales, demonstrating
354 robust generalization across architectures and model sizes.

355 Table 5 presents additional results on recent state-of-the-art
356 models, HunyuanVideo and Wan2.1. ANSE achieves con-
357 sistent improvements across quality metrics, underscoring
358 its plug-and-play applicability to a wide spectrum of video
359 diffusion models—from U-Net to MMDiT, and from mid-
360 scale to the latest state-of-the-art systems. [The statistical
361 significance analysis of these are provided in Appendix J.](#)

362 We further evaluate motion quality using the Fréchet Video
363 Motion Distance (FVMD) (Liu et al., 2024) on MSR-VTT (Xu et al., 2016), as shown in Table 6. We
364 sample 200 text prompts from the test split and generate videos with ANSE, using the corresponding
365 real videos as the reference distribution. ANSE consistently obtains lower FVMD scores, indicating
366 improved motion fidelity and reinforcing the motion-related gains observed in VBench.

367 **Qualitative Comparison.** Figure 4 presents representative qualitative comparisons on CogVideoX-
368 2B, CogVideoX-5B, and Wan2.1 with and without ANSE. Our approach consistently enhances
369 semantic fidelity, motion realism, and visual clarity across diverse prompts. For example, in separate
370 prompts such as “exploding” and “descends gracefully”, ANSE captures critical semantic transi-
371 tions—generating visible explosions in the former and preserving smooth temporal continuity in the
372 latter. In other prompts like “koala playing the piano” and “tasting beer”, it produces anatomically
373 coherent bodies with natural, expressive motion. These examples highlight ANSE’s ability to im-
374 prove spatial-temporal fidelity while generalizing effectively to large-scale video diffusion models.
375 Additional qualitative results, including other backbones, are provided in Appendix L.

376 **Computational Cost.** As shown in Table 4 and Table 5, ANSE introduces only a minimal increase
377 in inference time while delivering consistent quality gains. On AnimateDiff, inference time increases
378 by just +10.98%, compared to more than +105% when combined with FreqPrior and over +200%

341 Table 6: Comparison with FVMD met-
342 rics on MSRVTT dataset.

Backbone Model	Methods	FVMD ↓
HunyuanVideo (Kong et al., 2024)	Vanilla	17641.19
	+ Ours	16491.68
Wan2.1(1.3B) (Team, 2025)	Vanilla	16495.59
	+ Ours	14306.19

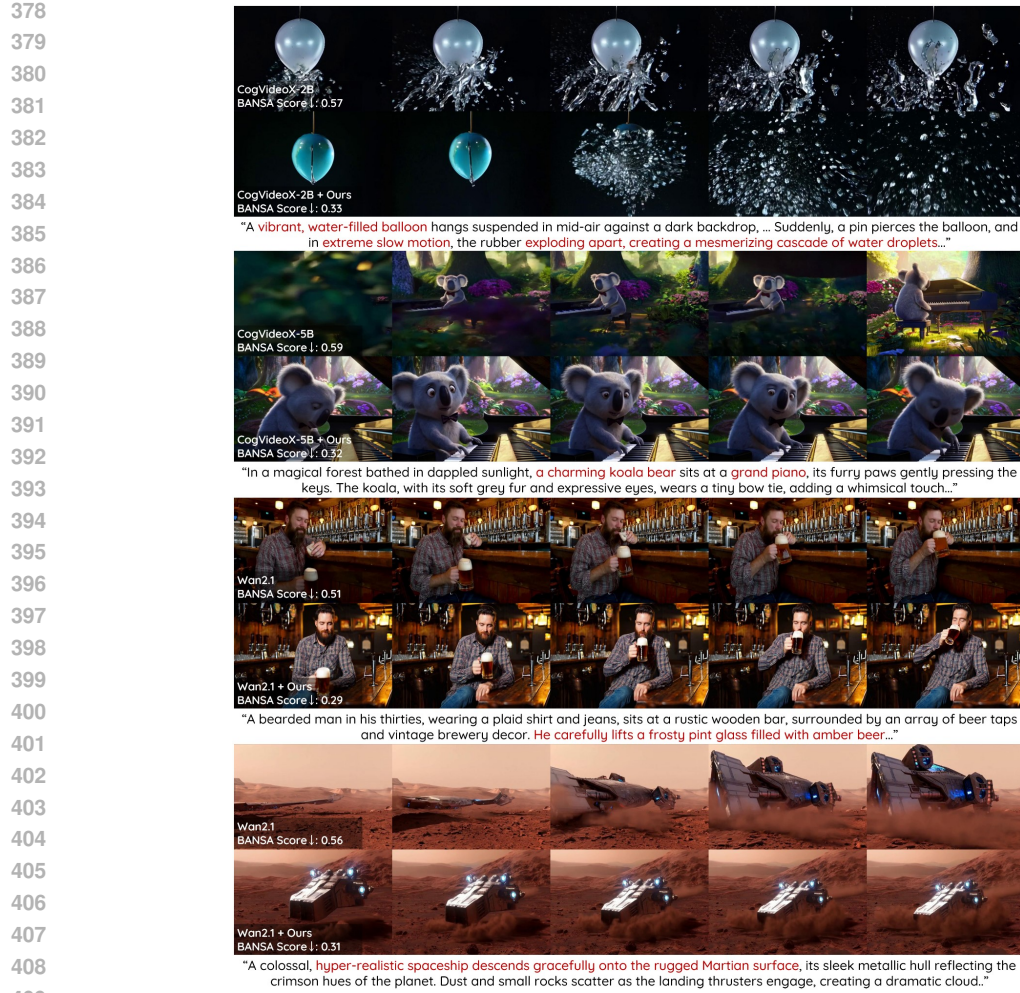


Figure 4: **Qualitative comparison with and without ANSE.** (CogvideoX-2B, 5B and Wan2.1). With ANSE, videos exhibit improved visual quality, better text alignment, and smoother motion transitions compared to the baseline. **White numbers show BANSA scores for the same prompt.**

for FreeInit. On CogVideoX models, the overhead is similarly small: +8% on the 2B variant and +13% on the 5B variant. For more recent architectures, ANSE adds only +14% on HunyuanVideo and +15% on Wan2.1. The overhead comes only from seed evaluation and leaves the sampling process and memory usage unchanged. In contrast, FreeInit and FreqPrior require multiple full passes, causing large slowdowns. ANSE improves quality across diverse backbones while keeping inference overhead below +15%, making it a practical plug-and-play solution for video diffusion.

6 ABLATION STUDY

Comparison of Acquisition Functions. Using CogVideoX-2B, we compare BANSA with random sampling, entropy-based selection, and two variants: BANSA (B) with Bernoulli masking and BANSA (D) with dropout-based stochasticity (Table 7). All methods improve over the baseline, but BANSA (B) consistently achieves the best scores across quality, semantic, and total metrics. This suggests that Bernoulli masking better captures attention-level uncertainty than dropout, underscoring the importance of modeling uncertainty in line with the model’s structure.

Effect of Ensemble Size K . We investigate how the number of stochastic forward passes K influences subject and background consistency (Table 8). Both metrics improve as K increases from 1 to 10, indicating that larger ensembles provide more reliable noise evaluation. Performance saturates at $K = 10$, which we set as the default in all experiments.

432
433 **Table 7: Comparison of different acquisition**
434 **functions for noise selection.**

Method	Quality Score	Semantic Score	Total Score
Random	82.08	76.83	81.03
Entropy	82.23	76.73	81.13
BANSA (D)	82.43	76.91	81.33
BANSA (B)	82.56	78.06	81.66

435 **Table 8: Effect of varying the number of K .**

K	Subject Consistency	Background Consistency
1	0.9618	0.9788
3	0.9623	0.9793
5	0.9632	0.9798
7	0.9638	0.9802
10	0.9641	0.9811

436 **Table 9: Quantitative comparison of reversed BANSA scoring on CogVideoX-2B.** This presents
437 results when selecting samples using the highest BANSA scores, compared to the default selection.

Method	Subject Consistency	Background Consistency	Temporal Flickering	Motion Smoothness	Aesthetic Quality	Imaging Quality	Dynamic Degree	Quality Score
Vanilla	0.9616	0.9788	0.9715	0.9743	0.6195	0.6267	0.6380	82.08
+ Ours (reverse)	0.9626	0.9785	0.9700	0.9741	0.6181	0.6253	0.6328	81.93
+ Ours	0.9641	0.9811	0.9775	0.9746	0.6202	0.6276	0.6511	82.56

438 **Table 10: Component analysis of Bernoulli masking parameters on Wan2.1 1.3B.**

Backbone Model	Bernoulli p	Subject Consistency \uparrow	Motion Smoothness \uparrow	Aesthetic Quality \uparrow	Imaging Quality \uparrow	Overall Consistency \uparrow
	0.0	0.9254	0.9751	0.6464	0.6459	0.2731
Wan2.1 1.3B	0.2	0.9310	0.9786	0.6559	0.6516	0.2763
	0.5	0.9308	0.9779	0.6543	0.6533	0.2727
	0.7	0.9302	0.9778	0.6557	0.6529	0.2726
	1.0	0.9232	0.9753	0.6451	0.6508	0.2721

439 **Table 11: Quantitative evaluation on the IPOC-2B after post-training and Wan2.1 14B model.**

Backbone Model	Method	Subject Consistency \uparrow	Background Consistency \uparrow	Temporal Flickering \uparrow	Motion Smoothness \uparrow	Aesthetic Quality \uparrow	Imaging Quality \uparrow	Dynamic Degree \uparrow
IPOC-2B	Vanilla	0.9273	0.9535	0.9918	0.9741	0.6554	0.664	0.7527
	+ Ours	0.9281	0.9534	0.9921	0.9745	0.6561	0.6644	0.7721
Wan2.1 14B	Vanilla	0.9290	0.9587	0.9931	0.9759	0.6572	0.6552	0.5916
	+ Ours	0.9302	0.9596	0.9938	0.9772	0.6601	0.6529	0.6277

460 **Effect of Noise Pool Size M .** We analyze the effect of noise pool size M , which controls the diversity
461 of candidate seeds in BANSA. Larger M improves the chance of finding high-quality seeds but
462 increases inference cost. As shown in Figure 8 (Appendix), performance saturates around $M = 10$
463 for CogVideoX-2B and -5B, which we adopt as the default for each model.

464 **Reversing the BANSA Criterion.** To further validate BANSA, we conduct a control experiment
465 where the noise seed with the *highest* BANSA score is selected—i.e., choosing the seed associated
466 with the greatest model uncertainty. As shown in Table 9, this reversal results in degradation of
467 quality-related metrics, confirming that lower BANSA scores are predictive of perceptually stronger
468 generations and supporting the validity of our selection strategy.

469 **Effect of Bernoulli masking probability p .** We conduct a sensitivity analysis on the Bernoulli
470 masking probability p using the Wanx 2.1 (1.3B) model. As shown in Table 10, both disabling
471 masking ($p = 0$) and fully random masking ($p = 1$) degrade performance, indicating that the masking
472 probability has a meaningful impact on the results. The method remains stable within the intermediate
473 range $p \in [0.2, 0.7]$, where overall performance varies only slightly. Among these configurations,
474 $p = 0.2$ delivers the best performance, which supports our choice of the default setting.

476 **Evaluation on strong video backbones and post-RL models.** We further evaluate our method on
477 stronger settings, including the large-capacity Wan2.1 14B backbone and the post-trained IPOC-2B
478 model. IPOC-2B is refined with a DPO-related preference alignment method (Yang et al., 2025),
479 making it a competitive post-RL baseline. As shown in Table 11, our method consistently improves
480 over the vanilla models across most VBench dimensions, demonstrating generalization to larger
481 architectures and robustness under preference-aligned post-RL training.

483 **User Study.** We conducted a human preference study in which evaluators compared paired videos
484 generated with and without our method along two criteria: overall quality and text-video alignment.
485 As shown in Fig. 5 (a), our method is consistently preferred on both aspects, indicating improvements
in perceptual quality and semantic alignment. The details are provided in Appendix K.

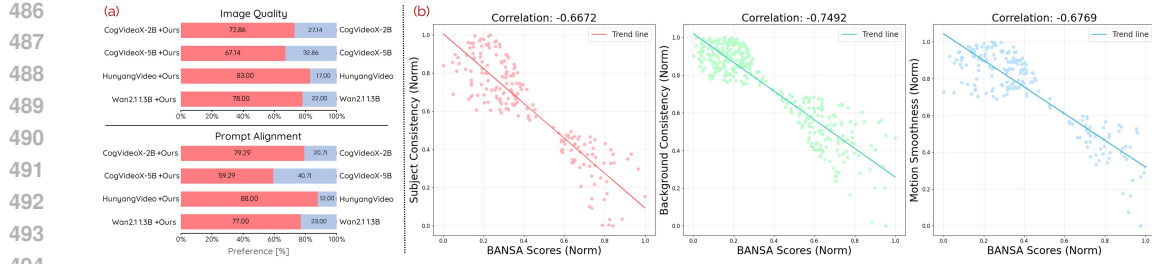


Figure 5: (a) User study showing consistent human preference for our method in overall quality and text-video alignment. (b) Correlation analysis where BANSA scores exhibit strong negative trends with key VBench metrics, indicating that lower scores correspond to higher-quality generations.



Figure 6: **Failure case and limitation of our method.** Although the BANSA score indicates low uncertainty, the resulting video still contains unnatural content. This represent a limitation of ours: we select optimal seeds but do not alter the generation process itself.

Analysis on correlation with actual quality. We examined how BANSA scores relate to quality by sampling diverse prompts and noise inputs and visualizing their score-quality trends in Fig. 5(b). Pearson correlations show strong negative relationships with Subject Consistency (-0.6672), Background Consistency (-0.7492), and Motion Smoothness (-0.6769), indicating that lower BANSA scores reliably associate with higher-quality and more stable generations.

7 DISCUSSION AND LIMITATIONS

Our method focuses on noise–seed selection based on model uncertainty, which introduces several limitations. As shown in Figure 6, even seeds with low BANSA scores may still produce unnatural results because ANSE does not modify the subsequent sampling process. Moreover, BANSA captures uncertainty at the attention level, which does not fully account for semantic or aesthetic quality. Although evaluating multiple candidates with stronger quality metrics could reduce this gap, such an approach is computationally prohibitive. A promising direction for future work is to integrate ANSE with post-training refinement methods—such as Self-Forcing (SF) (Huang et al., 2025)—that directly enhance sample quality. Notably, ANSE already works effectively with post-RL refinement methods like IPoC, and extending this compatibility to SF represents a natural next step. Such combinations may yield complementary gains in both quality and robustness beyond seed selection alone.

8 CONCLUSION

We present ANSE, a framework for active noise selection in video diffusion models. At its core is BANSA, an acquisition function that leverages attention-derived uncertainty to identify noise seeds yielding confident, consistent attention and thus higher-quality generations. BANSA adapts the BALD principle to the generative setting by operating in attention space, with efficient deployment enabled through Bernoulli-masked attention and lightweight layer selection. Experiments across multiple T2V backbones show that ANSE improves video quality and prompt alignment with minimal inference overhead. This introduces an inference-time scaling paradigm, enhancing generation not by altering the model or sampling steps, but through informed seed selection.

540 REFERENCES
541

542 Andreas Blattmann, Robin Rombach, Huan Ling, Tim Dockhorn, Seung Wook Kim, Sanja Fidler,
543 and Karsten Kreis. Align your latents: High-resolution video synthesis with latent diffusion
544 models. In *Proceedings of the IEEE/CVF conference on computer vision and pattern recognition*,
545 pp. 22563–22575, 2023.

546 Bradley Brown, Jordan Juravsky, Ryan Ehrlich, Ronald Clark, Quoc V Le, Christopher Ré, and
547 Azalia Mirhoseini. Large language monkeys: Scaling inference compute with repeated sampling.
548 *arXiv preprint arXiv:2407.21787*, 2024.

549 Haoxin Chen, Menghan Xia, Yingqing He, Yong Zhang, Xiaodong Cun, Shaoshu Yang, Jinbo Xing,
550 Yaofang Liu, Qifeng Chen, Xintao Wang, Chao Weng, and Ying Shan. Videocrafter1: Open
551 diffusion models for high-quality video generation, 2023.

552 Haoxin Chen, Yong Zhang, Xiaodong Cun, Menghan Xia, Xintao Wang, Chao Weng, and Ying
553 Shan. Videocrafter2: Overcoming data limitations for high-quality video diffusion models. In
554 *Proceedings of the IEEE/CVF Conference on Computer Vision and Pattern Recognition*, pp.
555 7310–7320, 2024a.

556 Junsong Chen, Chongjian Ge, Enze Xie, Yue Wu, Lewei Yao, Xiaozhe Ren, Zhongdao Wang, Ping
557 Luo, Huchuan Lu, and Zhenguo Li. Pixart- σ : Weak-to-strong training of diffusion transformer for
558 4k text-to-image generation. In *European Conference on Computer Vision*, pp. 74–91. Springer,
559 2024b.

560 Sherry X Chen, Yaron Vaxman, Elad Ben Baruch, David Asulin, Aviad Moreshet, Kuo-Chin Lien,
561 Misha Sra, and Pradeep Sen. Tino-edit: Timestep and noise optimization for robust diffusion-based
562 image editing. In *Proceedings of the IEEE/CVF Conference on Computer Vision and Pattern
563 Recognition*, pp. 6337–6346, 2024c.

564 Bradley Efron. Tweedie’s formula and selection bias. *Journal of the American Statistical Association*,
565 106(496):1602–1614, 2011.

566 Patrick Esser, Sumith Kulal, Andreas Blattmann, Rahim Entezari, Jonas Müller, Harry Saini, Yam
567 Levi, Dominik Lorenz, Axel Sauer, Frederic Boesel, et al. Scaling rectified flow transformers for
568 high-resolution image synthesis. In *Forty-first international conference on machine learning*, 2024.

569 Luca Eyring, Shyamgopal Karthik, Karsten Roth, Alexey Dosovitskiy, and Zeynep Akata. Reno:
570 Enhancing one-step text-to-image models through reward-based noise optimization. *Advances in
571 Neural Information Processing Systems*, 37:125487–125519, 2024.

572 Yarin Gal, Riashat Islam, and Zoubin Ghahramani. Deep bayesian active learning with image data.
573 In *International conference on machine learning*, pp. 1183–1192. PMLR, 2017.

574 Songwei Ge, Seungjun Nah, Guilin Liu, Tyler Poon, Andrew Tao, Bryan Catanzaro, David Jacobs,
575 Jia-Bin Huang, Ming-Yu Liu, and Yogesh Balaji. Preserve your own correlation: A noise prior for
576 video diffusion models. In *Proceedings of the IEEE/CVF International Conference on Computer
577 Vision*, pp. 22930–22941, 2023.

578 Xiefan Guo, Jinlin Liu, Miaomiao Cui, Jiankai Li, Hongyu Yang, and Di Huang. Initno: Boosting
579 text-to-image diffusion models via initial noise optimization. In *Proceedings of the IEEE/CVF
580 Conference on Computer Vision and Pattern Recognition*, pp. 9380–9389, 2024a.

581 Yuwei Guo, Ceyuan Yang, Anyi Rao, Zhengyang Liang, Yaohui Wang, Yu Qiao, Maneesh Agrawala,
582 Dahua Lin, and Bo Dai. Animatediff: Animate your personalized text-to-image diffusion models
583 without specific tuning. *International Conference on Learning Representations*, 2024b.

584 Yoav HaCohen, Nisan Chiprut, Benny Brazowski, Daniel Shalem, Dudu Moshe, Eitan Richardson,
585 Eran Levin, Guy Shiran, Nir Zabari, Ori Gordon, et al. Ltx-video: Realtime video latent diffusion.
586 *arXiv preprint arXiv:2501.00103*, 2024.

587 Yingqing He, Tianyu Yang, Yong Zhang, Ying Shan, and Qifeng Chen. Latent video diffusion models
588 for high-fidelity long video generation. 2022.

594 Jonathan Ho, Ajay Jain, and Pieter Abbeel. Denoising diffusion probabilistic models. *Advances in*
 595 *neural information processing systems*, 33:6840–6851, 2020.

596

597 Wenyi Hong, Ming Ding, Wendi Zheng, Xinghan Liu, and Jie Tang. Cogvideo: Large-scale
 598 pretraining for text-to-video generation via transformers. *arXiv preprint arXiv:2205.15868*, 2022.

599

600 Neil Houlsby, Ferenc Huszár, Zoubin Ghahramani, and Máté Lengyel. Bayesian active learning for
 601 classification and preference learning. *arXiv preprint arXiv:1112.5745*, 2011.

602

603 Xun Huang, Zhengqi Li, Guande He, Mingyuan Zhou, and Eli Shechtman. Self forcing: Bridging
 604 the train-test gap in autoregressive video diffusion. *arXiv preprint arXiv:2506.08009*, 2025.

605

606 Ziqi Huang, Yinan He, Jiashuo Yu, Fan Zhang, Chenyang Si, Yuming Jiang, Yuanhan Zhang, Tianxing
 607 Wu, Qingyang Jin, Nattapol Champaisit, Yaohui Wang, Xinyuan Chen, Limin Wang, Dahua Lin,
 608 Yu Qiao, and Ziwei Liu. VBench: Comprehensive benchmark suite for video generative models.
 609 In *Proceedings of the IEEE/CVF Conference on Computer Vision and Pattern Recognition*, 2024.

610

611 Kwanyoung Kim and Jong Chul Ye. Noise2score: Tweedie’s approach to self-supervised image
 612 denoising without clean images. *Advances in Neural Information Processing Systems*, 34:864–874,
 613 2021.

614

615 Kwanyoung Kim, Dongwon Park, Kwang In Kim, and Se Young Chun. Task-aware variational
 616 adversarial active learning. In *Proceedings of the IEEE/CVF conference on computer vision and*
 617 *pattern recognition*, pp. 8166–8175, 2021.

618

619 Andreas Kirsch, Joost Van Amersfoort, and Yarin Gal. Batchbald: Efficient and diverse batch
 620 acquisition for deep bayesian active learning. *Advances in neural information processing systems*,
 621 32, 2019.

622

623 Weijie Kong, Qi Tian, Zijian Zhang, Rox Min, Zuozhuo Dai, Jin Zhou, Jiangfeng Xiong, Xin Li,
 624 Bo Wu, Jianwei Zhang, et al. Hunyuandvideo: A systematic framework for large video generative
 625 models. *arXiv preprint arXiv:2412.03603*, 2024.

626

627 Jiahe Liu, Youran Qu, Qi Yan, Xiaohui Zeng, Lele Wang, and Renjie Liao. Fr\’echet video motion
 628 distance: A metric for evaluating motion consistency in videos. *arXiv preprint arXiv:2407.16124*,
 2024.

629

630 Nanye Ma, Shangyuan Tong, Haolin Jia, Hexiang Hu, Yu-Chuan Su, Mingda Zhang, Xuan Yang,
 631 Yandong Li, Tommi Jaakkola, Xuhui Jia, et al. Inference-time scaling for diffusion models beyond
 632 scaling denoising steps. *arXiv preprint arXiv:2501.09732*, 2025.

633

634 Oisin Mac Aodha, Neill DF Campbell, Jan Kautz, and Gabriel J Brostow. Hierarchical subquery
 635 evaluation for active learning on a graph. In *Proceedings of the IEEE conference on computer*
 636 *vision and pattern recognition*, pp. 564–571, 2014.

637

638 Karl Pearson. Notes on regression and inheritance in the case of two parents. *Proceedings of the*
 639 *Royal Society of London*, pp. 337–344, 1895.

640

641 Haonan Qiu, Menghan Xia, Yong Zhang, Yingqing He, Xintao Wang, Ying Shan, and Ziwei Liu.
 642 Freenoise: Tuning-free longer video diffusion via noise rescheduling. In *The Twelfth International*
 643 *Conference on Learning Representations*.

644

645 Robin Rombach, Andreas Blattmann, Dominik Lorenz, Patrick Esser, and Björn Ommer. High-
 646 resolution image synthesis with latent diffusion models. In *Proceedings of the IEEE/CVF confer-*
 647 *ence on computer vision and pattern recognition*, pp. 10684–10695, 2022.

648

649 Ozan Sener and Silvio Savarese. Active learning for convolutional neural networks: A core-set
 650 approach. *arXiv preprint arXiv:1708.00489*, 2017.

651

652 Claude E Shannon. A mathematical theory of communication. *Bell system technical journal*, 27(3):
 653 379–423, 1948.

654

655 Samarth Sinha, Sayna Ebrahimi, and Trevor Darrell. Variational adversarial active learning. In
 656 *Proceedings of the IEEE/CVF international conference on computer vision*, pp. 5972–5981, 2019.

648 Charlie Snell, Jaehoon Lee, Kelvin Xu, and Aviral Kumar. Scaling llm test-time compute optimally
 649 can be more effective than scaling model parameters. *arXiv preprint arXiv:2408.03314*, 2024.
 650

651 Jiaming Song, Chenlin Meng, and Stefano Ermon. Denoising diffusion implicit models. In *ICLR*,
 652 2021a.

653 Yang Song, Jascha Sohl-Dickstein, Diederik P. Kingma, Abhishek Kumar, Stefano Ermon, and Ben
 654 Poole. Score-based generative modeling through stochastic differential equations. In *ICLR*, 2021b.
 655

656 Wan Team. Wan: Open and advanced large-scale video generative models. 2025.

657 Toan Tran, Thanh-Toan Do, Ian Reid, and Gustavo Carneiro. Bayesian generative active deep learning.
 658 In *International conference on machine learning*, pp. 6295–6304. PMLR, 2019.
 659

660 Pascal Vincent. A connection between score matching and denoising autoencoders. *Neural computa-*
 661 *tion*, 23(7):1661–1674, 2011.

662 Jiuniu Wang, Hangjie Yuan, Dayou Chen, Yingya Zhang, Xiang Wang, and Shiwei Zhang. Mod-
 663 ellscope text-to-video technical report. *arXiv preprint arXiv:2308.06571*, 2023.
 664

665 Yaohui Wang, Xinyuan Chen, Xin Ma, Shangchen Zhou, Ziqi Huang, Yi Wang, Ceyuan Yang, Yinan
 666 He, Jiashuo Yu, Peiqing Yang, et al. Lavie: High-quality video generation with cascaded latent
 667 diffusion models. *International Journal of Computer Vision*, 133(5):3059–3078, 2025.

668 Tianxing Wu, Chenyang Si, Yuming Jiang, Ziqi Huang, and Ziwei Liu. Freeinit: Bridging initializa-
 669 tion gap in video diffusion models. In *European Conference on Computer Vision*, pp. 378–394.
 670 Springer, 2024.

671 Enze Xie, Junsong Chen, Junyu Chen, Han Cai, Haotian Tang, Yujun Lin, Zhekai Zhang, Muyang Li,
 672 Ligeng Zhu, Yao Lu, et al. Sana: Efficient high-resolution image synthesis with linear diffusion
 673 transformers. *arXiv preprint arXiv:2410.10629*, 2024.

674 Jun Xu, Tao Mei, Ting Yao, and Yong Rui. Msr-vtt: A large video description dataset for bridging
 675 video and language. In *Proceedings of the IEEE conference on computer vision and pattern*
 676 *recognition*, pp. 5288–5296, 2016.

677 Katherine Xu, Lingzhi Zhang, and Jianbo Shi. Good seed makes a good crop: Discovering secret
 678 seeds in text-to-image diffusion models. In *2025 IEEE/CVF Winter Conference on Applications of*
 679 *Computer Vision (WACV)*, pp. 3024–3034. IEEE, 2025.

680 Xiaomeng Yang, Zhiyu Tan, and Hao Li. Ipo: Iterative preference optimization for text-to-video
 681 generation. *arXiv preprint arXiv:2502.02088*, 2025.

682 Yi Yang, Zhigang Ma, Feiping Nie, Xiaojun Chang, and Alexander G Hauptmann. Multi-class active
 683 learning by uncertainty sampling with diversity maximization. *International Journal of Computer*
 684 *Vision*, 113:113–127, 2015.

685 Zhuoyi Yang, Jiayan Teng, Wendi Zheng, Ming Ding, Shiyu Huang, Jiazheng Xu, Yuanming Yang,
 686 Wenyi Hong, Xiaohan Zhang, Guanyu Feng, et al. Cogvideox: Text-to-video diffusion models
 687 with an expert transformer. *arXiv preprint arXiv:2408.06072*, 2024.

688 Donggeun Yoo and In So Kweon. Learning loss for active learning. In *Proceedings of the IEEE/CVF*
 689 *conference on computer vision and pattern recognition*, pp. 93–102, 2019.

690 Yunlong Yuan, Yuanfan Guo, Chunwei Wang, Wei Zhang, Hang Xu, and Li Zhang. Freqprior:
 691 Improving video diffusion models with frequency filtering gaussian noise. *arXiv preprint*
 692 *arXiv:2502.03496*, 2025.

693 Zangwei Zheng, Xiangyu Peng, Tianji Yang, Chenhui Shen, Shenggui Li, Hongxin Liu, Yukun Zhou,
 694 Tianyi Li, and Yang You. Open-sora: Democratizing efficient video production for all. *arXiv*
 695 *preprint arXiv:2412.20404*, 2024.

696

697

698

699

700

701

702 **A SUPPLEMENTARY SECTION**
703704 In this supplementary document, we present the following:
705

- 706 • Proof of Proposition 1 from the main paper regarding the BANSA Zero condition in
707 Section B.
- 708 • Implementation details of ANSE and evaluation metrics in Section C.
- 709 • Further explanation of layer selection through cumulative BANSA correlation in Section D.
- 710 • Additional ablation studies, including full-layer BANSA score analysis (Section E), temporal
711 scope effects (Section F), and attention-space effects (Section G).
- 712 • Additional analysis, including effect of CFG scale (Section H), equivalent computation
713 budget (Section I), statistical validation (Section J), and user study protocol (Section K).
- 714 • Additional qualitative results demonstrating the impact of BANSA Score in Section L.

718 **B PROOF OF PROPOSITION 1**
719720 **Proposition 1** (BANSA Zero Condition). *Let $\mathcal{A}(\mathbf{z}, c, t) = \{A^{(1)}, \dots, A^{(K)}\}$ be a set of row-
721 stochastic attention maps. Then:*

722
$$\text{BANSA}(\mathbf{z}, c, t) = 0 \Leftrightarrow A^{(1)} = \dots = A^{(K)}.$$

723

725 *Proof.* BANSA is defined as the difference between the average entropy and the entropy of the
726 average:

727
$$\text{BANSA}(\mathbf{z}, c, t) = \mathcal{H}\left(\frac{1}{K} \sum_{k=1}^K A^{(k)}(\mathbf{z}, c, t)\right) - \frac{1}{K} \sum_{k=1}^K \mathcal{H}(A^{(k)}(\mathbf{z}, c, t)).$$

728

730 Since the Shannon entropy $\mathcal{H}(\cdot)$ is strictly concave over the probability simplex. Therefore, by
731 Jensen's inequality:

732
$$\mathcal{H}\left(\frac{1}{K} \sum_{k=1}^K A^{(k)}\right) \geq \frac{1}{K} \sum_{k=1}^K \mathcal{H}(A^{(k)}),$$

733

735 with equality if and only if $A^{(1)} = \dots = A^{(K)}$. Thus, $\text{BANSA}(\mathbf{z}, c, t) = 0$ if and only if all attention
736 maps are identical. \square
737738 **Remark 1.** (Interpretation) This result confirms that the BANSA score quantifies disagreement
739 among sampled attention maps. A BANSA score of zero occurs only when all stochastic attention
740 realizations collapse to a single deterministic map—i.e., the model exhibits **no epistemic uncertainty**
741 in its attention distribution. Higher BANSA values indicate greater variation across samples, and thus,
742 higher uncertainty. In this sense, BANSA acts as a Jensen–Shannon-type divergence over attention
743 maps, capturing their dispersion under stochastic masking.745 **C FURTHER DETAILS ON EVALUATION METRICS AND IMPLEMENTATION**
746747 **Evaluation Metrics** To evaluate performance on Vbench, we use the Vbench-long version, where
748 prompts are augmented using GPT-4o across all evaluation dimensions. This version is specifically
749 designed for assessing videos longer than 4 seconds.750 We rigorously evaluate our generated videos following the official evaluation protocol. The Quality
751 Score is a weighted average of the following aspects: subject consistency, background consistency,
752 temporal flickering, motion smoothness, aesthetic quality, imaging quality, and dynamic degree.
753754 The Semantic Score is a weighted average of the following semantic dimensions: object class,
755 multiple objects, human action, color, spatial relationship, scene, appearance style, temporal style,
and overall consistency.

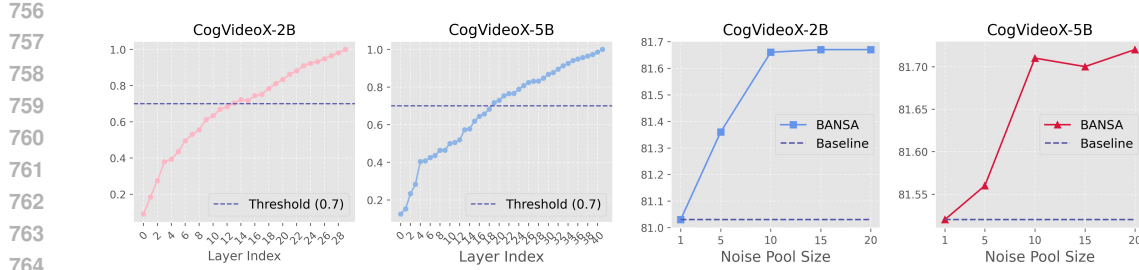


Figure 7: **Correlation analysis between cumulative BANSA score and full-layer scores.** We evaluate total scores across three text-to-video diffusion models with varying M , and select suitable values based on computational cost.

The Total Score is then computed as a weighted combination of the Quality Score and Semantic Score:

$$\text{Total Score} = \frac{w_1}{w_1 + w_2} \cdot \text{Quality Score} + \frac{w_2}{w_1 + w_2} \cdot \text{Semantic Score}$$

where $w_1 = 4$ and $w_2 = 1$, following the default setting in the official implementation.

Implementation We compute our BANSA score using the BALD-style formulation, which yields non-negative values. For clearer visualization, we normalize the BANSA scores from their original range (minimum: 0.45, maximum: 0.60) to the $[0, 1]$ interval. This normalization is used solely for visual clarity in figures and plots, and does not affect the noise selection process, which operates on the raw BANSA scores. [All models are evaluated using their default inference configurations: AnimateDiff \(50 steps\), CogVideo-X \(50 steps\), Wan2.1 \(50 steps\), and HunyuanVideo \(50 steps\).](#)

D FURTHER DETAIL OF BANSA LAYER-WISE CORRELATION ANALYSIS

Prompt construction. We evenly sampled 100 prompts from the four official VBench categories: *Subject Consistency*, *Overall Consistency*, *Temporal Flickering*, and *Scene*. Each category contains 25 prompts, selected to ensure diversity in motion, structure, and semantics.

Below are representative examples:

- *Subject Consistency* (e.g., “A young man with long, flowing hair sits on a rustic wooden stool in a cozy room, strumming an acoustic guitar...”)
- *Overall Consistency* (e.g., “A mesmerizing splash of turquoise water erupts in extreme slow motion, each droplet suspended in mid-air...”)
- *Temporal Flickering* (e.g., “A cozy restaurant with flickering candles and soft music. Patrons dine peacefully as snow falls outside...”)
- *Scene* (e.g., “A university campus transitions from lively student life to a golden sunset behind the clock tower...”)

Prompt sampling was stratified to ensure coverage of diverse visual and temporal patterns. The full list of prompts will be made publicly available upon code release.

BANSA score computation and correlation analysis. For each prompt, we generated 10 videos using different random noise seeds and computed BANSA scores at each attention layer. This yielded one full-layer BANSA score and a set of layer-wise scores per seed. To obtain stable estimates, we averaged the per-layer and full-layer BANSA scores across the 10 seeds, reducing noise-specific variance and capturing consistent uncertainty patterns.

We then computed Pearson correlations between the cumulative BANSA scores (summed from layer 1 to d) and the official quality scores. The optimal depth d^* was defined as the smallest d at which the correlation exceeded 0.7, a widely used threshold indicating a strong positive relationship. As shown in Figure 7, this point was reached at $d^* = 14$ for CogVideoX-2B and $d^* = 19$ for CogVideoX-5B.

810 For AnimateDiff, the correlation crossed the threshold earlier at $d^* = 10$, while for HunyuanVideo
 811 and Wanx 2.1 it consistently appeared around $d^* = 20$. These model-specific depths were applied
 812 throughout all experiments. Such consistency across architectures empirically supports our choice
 813 of the 0.7 threshold and ensures that the correlation analysis reflects generalizable, noise-agnostic
 814 patterns of attention-based uncertainty.

815 Table 12: Comparison between full-layer and truncated BANSA score.
 816

Backbone Model	Method	Subject Consistency ↑	Background Consistency ↑	Temporal Flickering ↑	Motion Smoothness ↑	Aesthetic Quality ↑	Imaging Quality ↑	Dynamic Degree ↑	Quality Score ↑	Inference Time ↓
CogVideoX-2B	Full-layer	0.9639	0.9810	0.9801	0.9743	0.6198	0.6244	0.6516	82.58	303.7
	Truncated	0.9641	0.9811	0.9775	0.9746	0.6202	0.6276	0.6511	82.56	269.3
CogvideoX-5B	Full-layer	0.9660	0.9630	0.9863	0.9708	0.6168	0.6290	0.6979	82.71	810.3
	Truncated	0.9658	0.9639	0.9861	0.9711	0.6179	0.6290	0.6918	82.70	754.3

823

E EFFECTIVENESS OF TRUNCATED BANSA SCORE

 824

825 To reduce the computational overhead of BANSA evaluation, we adopt a truncated score that
 826 aggregates attention uncertainty only up to a fixed depth d^* , rather than summing over all layers.
 827 To evaluate the effectiveness of this approximation, we compared the final generation quality when
 828 selecting noise seeds using either the full-layer or truncated BANSA scores.
 829

830 As shown in Table 12, both approaches yield highly similar results across all seven dimensions
 831 of the VBench evaluation protocol (subject consistency, background consistency, aesthetic quality,
 832 imaging quality, motion smoothness, dynamic degree, and temporal flickering). Importantly, the
 833 overall quality scores are preserved despite the substantial reduction in attention layers used.

834 This demonstrates that truncated BANSA is sufficient to capture the key uncertainty signals for
 835 reliable noise selection while reducing inference time. The strong alignment in quality stems from
 836 the fact that our method relies on relative ranking rather than absolute values, allowing for efficient
 837 yet robust selection with significantly lower computational cost. We attribute this effectiveness to
 838 the fact that most informative attention behaviors emerge early in the denoising process, allowing
 839 accurate uncertainty estimation without full-layer computation.

840 Table 13: Effect of temporal scope in BANSA score on generation quality.
 841

BANSA Scope	Subject Consistency ↑	Temporal Flickering ↑	Motion Smoothness ↑	Aesthetic Quality ↑	Imaging Quality ↑	Dynamic Degree ↑	Inference Time ↓
1-step	0.9639	0.9801	0.9743	0.6198	0.6244	0.6516	× 1
25-step avg	0.9651	0.9798	0.9746	0.6202	0.6271	0.6511	× 25
50-step avg	0.9652	0.9799	0.9751	0.6203	0.6276	0.6514	× 50

848

F EFFECT OF TEMPORAL SCOPE IN BANSA SCORE

 849

850 While our method computes the BANSA score only at the first denoising step to minimize cost, it is
 851 natural to ask whether incorporating more timesteps improves its predictive power for noise selection.
 852 To investigate this, we compute the average BANSA score across the first 1, 25, and 50 denoising
 853 steps and compare their effectiveness in predicting video quality.

854 Table 13 reports the VBench scores for subject consistency, aesthetic quality, imaging quality, motion
 855 smoothness, dynamic degree, and temporal flickering when using BANSA computed over different
 856 temporal scopes. Although using more timesteps results in slightly better quality, the gains are
 857 marginal. This indicates that most of the predictive signal for noise quality is embedded early in the
 858 generation trajectory.

859 More importantly, since BANSA is used solely to assess the uncertainty of the initial noise seed—not
 860 to track full-step generation behavior—our 1-step computation is sufficient to capture the core
 861 uncertainty signal. In contrast, computing BANSA over all steps requires running multiple attention
 862 forward passes across the full trajectory, resulting in substantial computational overhead that limits
 863 its practicality for real-world applications.

864

Table 14: Quantitative results on VBench using AnimateDiff, CogVideoX-2B and -5B.

865

866

867

868

869

870

871

872

873

874

875

876

877

878

879

880

881

882

883

884

G EFFECT OF ATTENTION SPACE IN BANSA SCORE

To further examine whether BANSA scores capture quality- or semantic-related uncertainty, we conducted additional experiments with the AnimateDiff backbone, which separates self- and cross-attention layers. Unlike CogVideo and Wanx, which adopt an MMDiT architecture where multimodal attention entangles both components, AnimateDiff provides a clearer lens for disentangling semantic effects. As shown in Table 14, applying BANSA to self-attention primarily improved perceptual quality scores, whereas applying it to cross-attention enhanced semantic alignment. This indicates that uncertainty over noise manifests differently depending on the attention type, supporting the interpretation that BANSA reflects both quality- and semantics-related variations. In contrast, MMDiT-based models such as CogVideo and Wanx integrate these dimensions within their unified attention structure, making them more suitable for overall noise selection in the main paper’s experiments.

Table 15: **Ablation study on the interaction between higher CFG scale and ours on Wan2.1(1.3B).**

Backbone Model	Method	CFG Scale	Subject Consistency ↑	Motion Smoothness ↑	Aesthetic Quality ↑	Imaging Quality ↑
Wanx 2.1 1.3B	Vanilla	5.0	0.9285	0.9748	0.6465	0.6519
	Ours	5.0	0.9310	0.9786	0.6559	0.6516
	Vanilla	7.5	0.9266	0.9740	0.6447	0.6357
	Ours	7.5	0.9276	0.9755	0.6519	0.6409

H EFFECT OF CFG SCALE ON OUR METHOD

Classifier-free guidance (CFG) modifies the conditional–unconditional interpolation only at the final stage of inference, whereas our method selects noise seeds at initialization based on attention-level uncertainty. Since they operate at different points in the pipeline, their effects are largely independent: CFG adjusts the extrapolation strength, while our method chooses seeds that lead to more stable early-stage behavior.

To assess potential interactions, we increased the CFG scale from the default value of 5.0 to 7.5 on the Wanx 2.1 (1.3B) model, as shown in Table 15. Higher CFG values generally degrade performance by pushing sampling beyond the model’s calibrated range. Nevertheless, our method consistently outperforms the vanilla baseline under both settings, indicating that its benefits remain stable across different CFG scales.

Table 16: **Ablation study under an equivalent computation budget. Increasing the baseline sampling steps does not consistently improve performance, whereas our method achieves better results with fewer effective steps.**

Backbone Model	Method	Steps	Subject Consistency ↑	Motion Smoothness ↑	Aesthetic Quality ↑	Imaging Quality ↑
Wan2.1 1.3B	Vanilla	50	0.9285	0.9748	0.6465	0.6519
	Vanilla	60	0.9274	0.9745	0.6476	0.6492
	Ours	< 60	0.9310	0.9786	0.6559	0.6516

918 I EFFECT OF EQUIVALENT COMPUTATION BUDGET

921 Our method evaluates $M = 10$ noise candidates, but the actual computation is lower than $50 + 10$
 922 steps because many candidates terminate early during partial denoising. To assess whether the
 923 baseline could benefit from additional computation, we increased its sampling steps from 50 to 60.
 924 As shown in Table 16, this results in only marginal changes and even degrades some metrics, likely
 925 because the model is not calibrated for longer sampling schedules.

926 In contrast, our method consistently improves performance while requiring fewer effective steps than
 927 the 60-step baseline, suggesting that the gains stem from selecting more stable noise initializations
 928 rather than from additional compute. This highlights the efficiency advantage of our approach under
 929 equivalent or lower computation budgets.

930 Table 17: Comparison of VBench Quality Scores With and Without BANSA. Scores are reported as
 931 mean (95% confidence interval, CI: lower – upper).

Backbone Model	Method	Subject Consistency ↑ (CI)	Background Consistency ↑ (CI)	Temporal Flickering ↑ (CI)	Motion Smoothness ↑ (CI)	Aesthetic Quality ↑ (CI)	Imaging Quality ↑ (CI)	Dynamic Degree ↑ (CI)
CogvideoX-2B	Baseline	0.9616 (0.9606 - 0.9626)	0.9788 (0.9779 - 0.9797)	0.9715 (0.9688 - 0.9742)	0.9738 (0.9733 - 0.9753)	0.6195 (0.6116 - 0.6274)	0.6267 (0.6160 - 0.6374)	0.6380 (0.6133 - 0.6627)
	+ Ours	0.9639 (0.9629 - 0.9649)	0.9810 (0.9795 - 0.9825)	0.9801 (0.9781 - 0.9821)	0.9743 (0.9737 - 0.9756)	0.6198 (0.6119 - 0.6277)	0.6244 (0.6137 - 0.6351)	0.6500 (0.6255 - 0.6745)
CogvideoX-5B	Baseline	0.9616 (0.9608 - 0.9624)	0.9616 (0.9602 - 0.9630)	0.9862 (0.9833 - 0.9891)	0.9712 (0.9703 - 0.9721)	0.6162 (0.6084 - 0.6240)	0.6272 (0.6170 - 0.6374)	0.6895 (0.6655 - 0.7135)
	+ Ours	0.9660 (0.9653 - 0.9667)	0.9630 (0.9616 - 0.9644)	0.9863 (0.9835 - 0.9891)	0.9708 (0.9700 - 0.9716)	0.6168 (0.6089 - 0.6247)	0.6290 (0.6189 - 0.6391)	0.6979 (0.6738 - 0.7220)

932 Table 18: Comparison of VBench Semantic Scores With and Without BANSA. Scores are reported
 933 as mean (95% confidence interval, CI: lower – upper).

Backbone Model	Method	Object Class ↑ (CI)	Multiple Object ↑ (CI)	Color ↑ (CI)	Spatial Relationship ↑ (CI)	Scene ↑ (CI)	Style ↑ (CI)	Temporal Consistency ↑ (CI)	Overall Consistency ↑ (CI)	Human Action ↑ (CI)	Appearance Style ↑ (CI)
CogvideoX-2B	Baseline	0.8522 (0.8511 - 0.8533)	0.6391 (0.6376 - 0.6406)	0.8318 (0.8302 - 0.8334)	0.7148 (0.6963 - 0.7333)	0.4815 (0.4801 - 0.4829)	0.2488 (0.2451 - 0.2523)	0.2722 (0.2679 - 0.2765)	0.9860 (0.9743 - 0.9977)	0.2397 (0.2483 - 0.2511)	
	+ Ours	0.8842 (0.8831 - 0.8853)	0.6596 (0.6581 - 0.6611)	0.8255 (0.8240 - 0.8270)	0.6915 (0.6728 - 0.7102)	0.5286 (0.5272 - 0.5300)	0.2547 (0.2511 - 0.2583)	0.2760 (0.2718 - 0.2802)	0.9870 (0.9757 - 0.9963)	0.2507 (0.2493 - 0.2521)	
CogvideoX-5B	Baseline	0.8595 (0.8585 - 0.8605)	0.6511 (0.6496 - 0.6526)	0.8218 (0.8202 - 0.8234)	0.6872 (0.6675 - 0.7069)	0.5233 (0.5219 - 0.5247)	0.2552 (0.2513 - 0.2591)	0.2761 (0.2717 - 0.2805)	0.9900 (0.9813 - 0.9987)	0.2483 (0.2354 - 0.2612)	
	+ Ours	0.8675 (0.8665 - 0.8685)	0.6658 (0.6643 - 0.6673)	0.8201 (0.8186 - 0.8216)	0.6831 (0.6637 - 0.7025)	0.5255 (0.5241 - 0.5269)	0.2585 (0.2546 - 0.2624)	0.2773 (0.2730 - 0.2816)	0.9980 (0.9910 - 1.0050)	0.2524 (0.2511 - 0.2537)	

934 Table 19: Comparison of VBench Quality Scores for HunyuanVideo and Wan2.1. Scores are reported
 935 as mean (95% confidence interval, CI: lower – upper).

Backbone Model	Method	Subject Consistency ↑ (CI)	Background Consistency ↑ (CI)	Motion Smoothness ↑ (CI)	Aesthetic Quality ↑ (CI)	Imaging Quality ↑ (CI)	Temporal Flickering ↑ (CI)
Hunyuan Video	Vanilla	0.9562 (0.9551 - 0.9573)	0.9656 (0.9645 - 0.9667)	0.9850 (0.9838 - 0.9862)	0.6276 (0.6198 - 0.6354)	0.6137 (0.6059 - 0.6215)	0.9921 (0.9902 - 0.9940)
	+ Ours	0.9612 (0.9603 - 0.9621)	0.9661 (0.9650 - 0.9672)	0.9858 (0.9847 - 0.9869)	0.6268 (0.6191 - 0.6345)	0.6151 (0.6075 - 0.6227)	0.9938 (0.9919 - 0.9957)
Wan2.1	Vanilla	0.9562 (0.9553 - 0.9571)	0.9656 (0.9644 - 0.9668)	0.9850 (0.9839 - 0.9861)	0.6276 (0.6201 - 0.6351)	0.6137 (0.6061 - 0.6213)	0.9943 (0.9924 - 0.9962)
	+ Ours	0.9612 (0.9601 - 0.9623)	0.9661 (0.9649 - 0.9673)	0.9858 (0.9846 - 0.9870)	0.6268 (0.6190 - 0.6346)	0.6151 (0.6073 - 0.6229)	0.9956 (0.9935 - 0.9977)

940 J STATISTICAL VALIDATION OF RESULTS

941 Our VBench evaluation uses 4,750 videos (five samples per prompt) across 17 fine-grained dimensions,
 942 where even small absolute gains are meaningful. To assess statistical significance, we computed
 943 95% confidence intervals using 10 independent runs, each based on random subsets of 100 videos. As
 944 shown in Tables 17, 18, and 19, our method consistently improves or maintains performance across
 945 quality-, semantic-, and motion-related metrics without exhibiting bias toward any particular subset.
 946 These statistical results provide strong evidence of the robustness and reliability of our approach.

947 K USER STUDY PROTOCOL

948 As presented in Fig. 5 (a), we conduct a human evaluation study to complement automated metrics
 949 and directly assess whether ANSE improves video quality and prompt coherence. We evaluate four
 950 representative video diffusion models—CogVideoX-2B, CogVideoX-5B, Wan 2.1, and Hunyuan-
 951 Video—by comparing their outputs with and without ANSE. To construct a fair evaluation protocol,
 952 we randomly sample 30 prompts from the *Subject Consistency* and *Overall Consistency* dimensions
 953 of the VBench benchmark. For each prompt, we generate paired videos using identical noise seeds
 954 for both the baseline and the ANSE-equipped models.

955 We recruit 12 independent human evaluators, all of whom remain fully blind to the models and are
 956 restricted to participating only once. Each evaluator is shown two videos side-by-side (baseline vs.
 957 ANSE) and responds to two questions:

1. **Video Quality:** “Which video appears more stable and visually pleasing?”
2. **Prompt Alignment:** “Which video better represents the given text prompt?”

972 The order of prompts and the arrangement of video pairs are fully randomized. Across all backbones
973 and prompts, models equipped with ANSE are consistently preferred in terms of both video quality
974 and prompt alignment, demonstrating the practical effectiveness and robustness of ANSE.
975

976 L ADDITIONAL QUALITATIVE COMPARISON 977

978 **More qualitative results.** Figures 9, 10, 11 12, and 13 present additional examples generated
979 using our noise selection framework including diverse backbone such as, AnimateDiff, CogVideoX2B
980 and 5B, HunyangVideo, and Wan2.1. Across diverse prompts, the selected seeds yield improved
981 spatial detail, aesthetic quality, and semantic alignment, further validating the robustness of our
982 approach. These examples complement our quantitative findings by illustrating the visual impact of
983 BANSA-based noise selection.
984

985 **Effect of BANSA score on generation quality.** Figures 14 provide a qualitative comparison of
986 outputs generated using three types of noise seeds: a randomly sampled seed, the seed with the
987 highest BANSA score (lowest quality), and the seed with the lowest BANSA score (highest quality).
988 All videos were generated using 50 denoising steps with the CogVideoX-5B backbone. The lowest-
989 BANSA seed consistently produces sharper, more coherent, and semantically faithful videos, whereas
990 the highest-BANSA seed often leads to structural artifacts or temporal instability. These results
991 highlight the practical value of BANSA-guided noise selection.
992
993
994
995
996
997
998
999
1000
1001
1002
1003
1004
1005
1006
1007
1008
1009
1010
1011
1012
1013
1014
1015
1016
1017
1018
1019
1020
1021
1022
1023
1024
1025

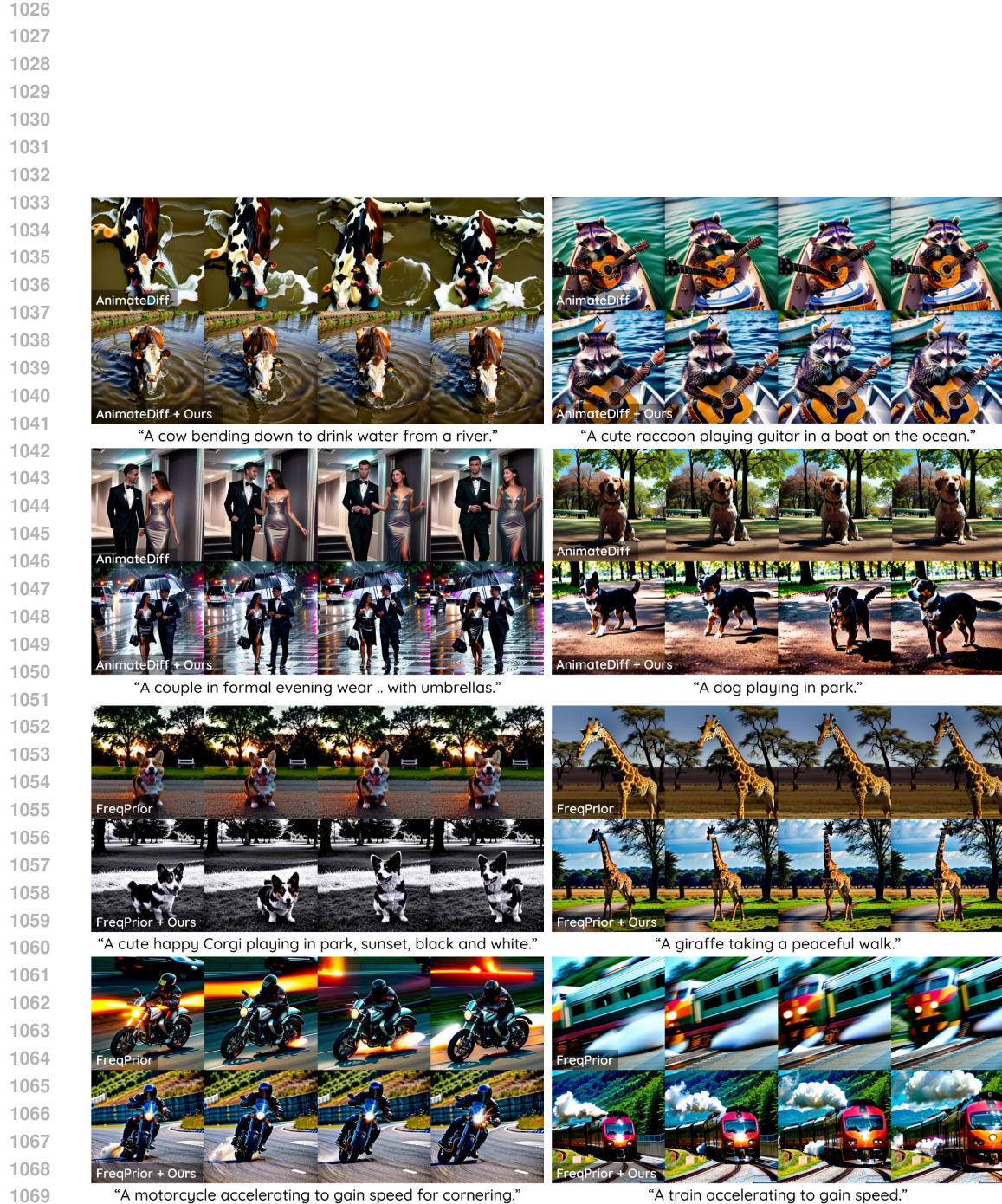


Figure 9: **Effect of ANSE on semantic fidelity and motion stability in AnimateDiff and FreqPrior.** Each block compares baseline generations with those using ANSE-selected noise. In addition, while FreqPrior serves as a noise-refinement baseline, our method is fully compatible and achieves further improvements when combined.

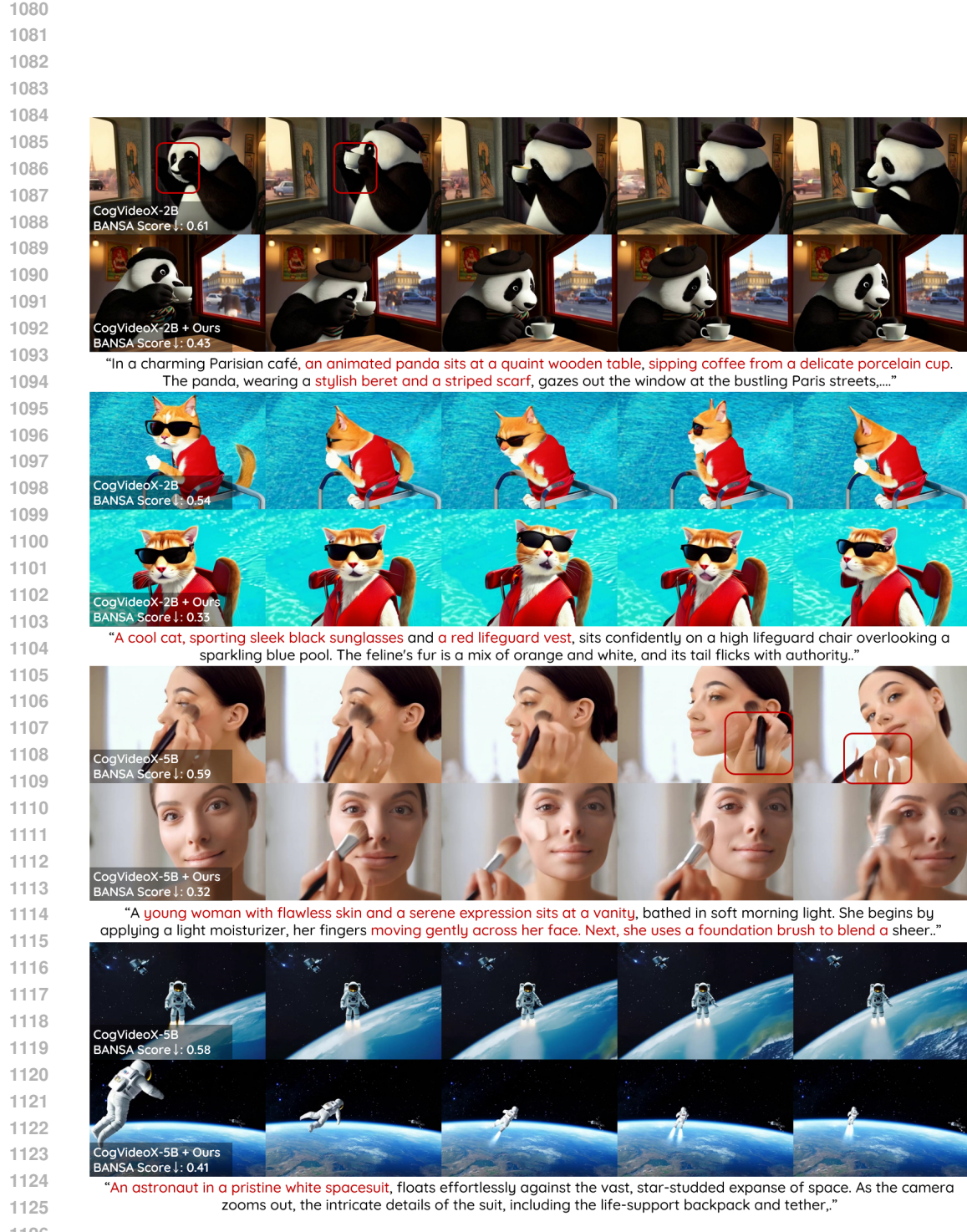


Figure 10: **Effect of ANSE on semantic fidelity and motion stability in CogVideoX outputs.** Each block compares baseline generations with those using ANSE-selected noise. Across both CogVideoX-2B and 5B, ANSE improves semantic alignment to the prompt and reduces artifacts such as temporal flickering and object distortion. **White numbers show BANSA scores for the same prompt.**

1134

1135

1136

1137

1138

1139

1140

1141

1142



1143

1144

1145

1146

1147

1148

"A sophisticated couple, dressed in elegant evening attire, walks down a dimly lit street, their formal. **The man, in a tailored black tuxedo, and the woman, in a flowing red gown, share a black umbrella as the rain captures their synchronized steps..**"

1149

1150

1151

1152

1153



1154

1155

1156

1157

1158

"A drone captures a breathtaking aerial view of a festive celebration in a snow-covered town square, centered around a towering, brilliantly lit Christmas tree adorned with twinkling lights and ornaments. The scene is alive with vibrant fireworks."

1159

1160

1161

1162

1163



1164

1165

1166

1167

1168

"In a whimsical forest clearing, a raccoon with a mischievous glint in its eye stands on a tree stump, holding an electric guitar. The raccoon, wearing a tiny leather jacket, strums the guitar with surprising skill, its tiny paws moving deftly over the strings...."

1169



1170

1171

1172

1173

1174

1175

1176

1177

1178

"A majestic elephant strolls gracefully through a lush, verdant forest, its massive feet gently pressing into the soft earth. The sunlight filters through the dense canopy, casting dappled shadows on its wrinkled, grey skin...."

1179

1180

1181

1182

1183

1184

1185

1186

1187

Figure 11: Additional qualitative comparison of CogVideoX variants with and without ANSE. Results from CogVideoX-2B are shown in the first two rows; the rest show CogVideoX-5B. With ANSE, videos exhibit improved visual quality, better text alignment, and smoother motion transitions compared to the baseline. **White numbers** show BANSA scores for the same prompt.

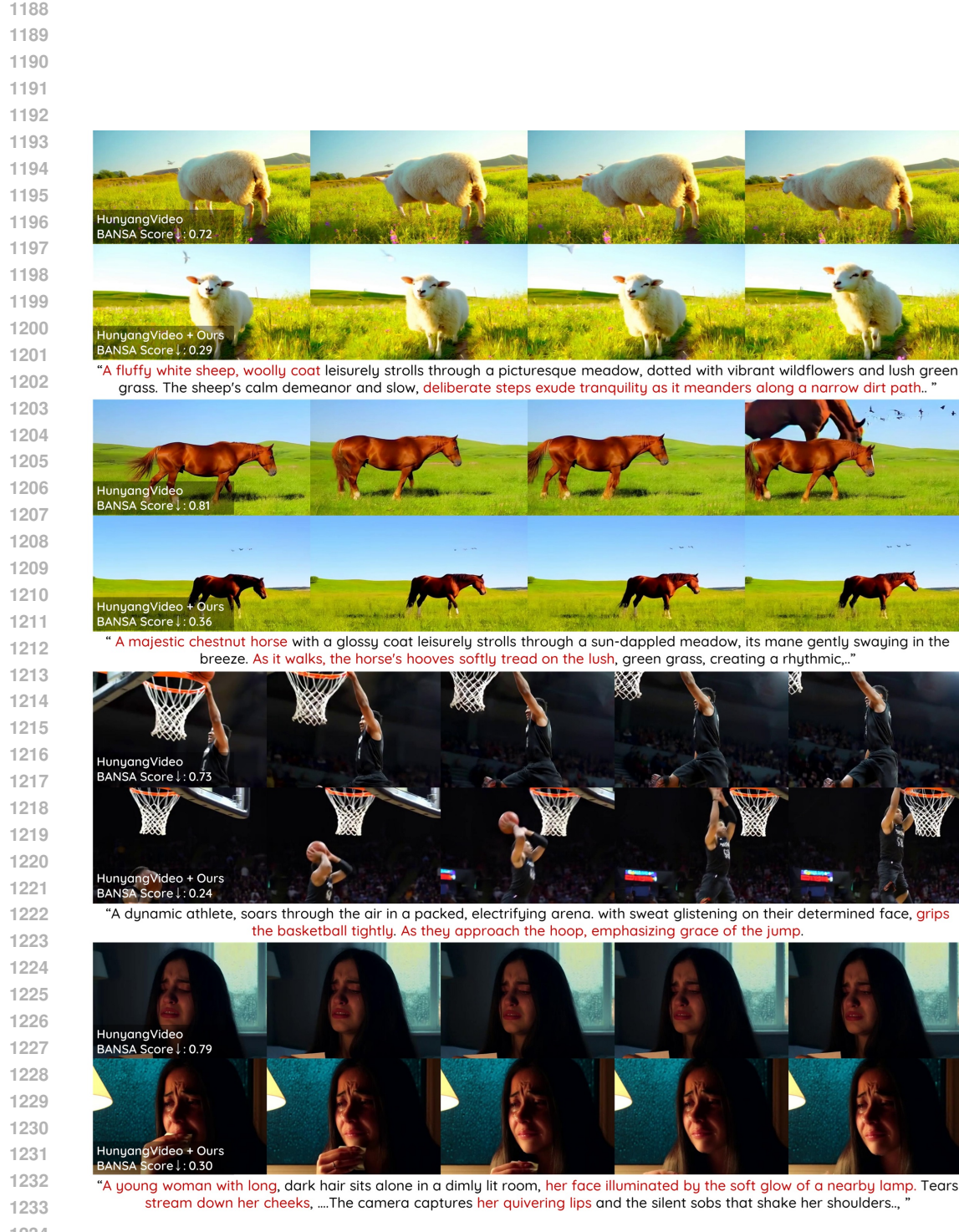


Figure 12: **Additional qualitative comparison of HunyangVideo with and without ANSE.** With ANSE, the generated videos achieve sharper visual fidelity, stronger alignment between text and content, and smoother motion progression than the baseline. **White numbers show BANSA scores for the same prompt.**

1242

1243

1244

1245

1246

1247

1248

1249

1250



1251

1252

1253

1254

1255

1256

"A determined individual in a sleek black tank top and gray athletic shorts performs push-ups on a pristine wooden floor in a minimalist, sunlit room. The camera captures the sweat glistening on their forehead, emphasizing their intense focus .."



1257

1258

1259

1260

1261

1262

1263

1264

1265

"A majestic steam train, with its vintage black and red carriages, chugs along a winding mountainside track, enveloped in a cloud of white steam. The train's powerful engine, adorned with brass accents, gleams in the sunlight as it ascends...."



1266

1267

1268

1269

1270

1271

1272

1273

1274

1275

1276

1277

"A vibrant, multi-colored ice cream cone sits on a rustic wooden table, its creamy swirls beginning to soften under the warm sunlight streaming through a nearby window. The camera zooms in to capture the intricate details of the melting ice cream"



1278

1279

1280

1281

1282

1283

1284

1285

1286

"A vibrant clownfish, with its striking orange and white stripes, gracefully navigates through a lush coral reef teeming with life. The fish weaves between the intricate branches of colorful corals, which range from deep purples to bright yellows,"

1287

1288

1289

1290

1291

1292

1293

1294

1295

1296

1297

1298

1299

1300

1301

1302

1303

1304

1305



1306

1307

1308

1309

1310

1311

1312

1313

1314

1315

1316

1317

1318

1319

1320

"A lone bicycle, with its sleek frame and black tires, glides effortlessly through a vast, snow-covered field under a pale winter sky. The rider, bundled in a red parka, black gloves, and a woolen hat, pedals steadily, leaving a delicate trail in the pristine snow. The scene captures the quiet serenity of the landscape, with snowflakes gently falling and the distant silhouette of bare trees lining the horizon. As the rider continues, the sun



1321

1322

1323

1324

1325

1326

1327

1328

1329

1330

1331

1332

1333

1334

1335

1336

"A majestic giraffe, its long neck gracefully arching, bends down to drink from a serene river, surrounded by lush greenery and tall grasses. The sun casts a golden glow, highlighting the giraffe's patterned coat and the gentle ripples in the water. Nearby, a family of zebras grazes peacefully, adding to the tranquil scene. Birds flutter above, their reflections dancing on the water's surface. The giraffe's delicate movements create a sense of harmony with nature, as the river flows gently, reflecting the vibrant colors of the surrounding landscape..."

1337

1338

1339

1340

1341

Figure 14: Qualitative comparison of generations from different noise seeds. We compare outputs generated from a randomly sampled seed (top), the seed with the highest BANSA score (middle), and the seed with the lowest score (bottom), using the same prompt and model. BANSA-selected seeds produce more coherent structure, stable motion, and stronger semantic alignment than both random and high-uncertainty seeds.

1342

1343

1344

1345

1346

1347

1348

1349